PHYSICAL REVIEW D **76,** 103001 (2007)

Excitable systems as robust event trigger generators in noisy detectors

M. Ciszak
C.N.R.– Istituto Nazionale di Ottica Applicata, Largo Enrico Fermi 6, I-50125 Firenze, Italy

M. Camarda
Dipartimento di Ingegneria dell'Informazione, Università di Padova, Via Gradenigo 6/B, I-35131 Padova, Italy, and INFN Laboratori Nazionali di Legnaro, Viale dell'Università 2, I-35020 Legnaro, Padova, Italy

F. Marino* and F. Marin
Dipartimento di Fisica, Università di Firenze and INFN Sezione di Firenze, Via Sansone 1, I-50019 Sesto Fiorentino, Firenze, Italy

A. Ortolan
INFN, Laboratori Nazionali di Legnaro, Viale dell'Università 2, I-35020 Legnaro, Padova, Italy
(Received 9 May 2007; published 12 November 2007)

We study the response of a stochastic FitzHugh-Nagumo model to weak external forcing with the aim of implementing a nonlinear algorithm, devised for the robust detection of transient signals such as gravitational wave bursts. In order to test the performance of the algorithm, we exploited the ensemble of maximum entropy signals—known as chirplets. In particular, we investigated the chirplet parameter subspace representing the gravitational wave bursts within range of nowadays interferometric detectors. We found that the false alarm rate can be controlled by changing the constant term in the equation of the slow variable while the detection efficiency is completely insensitive to the kind of injected chirplet. The receiver operating characteristic curves have been evaluated and compared with the performance of power detectors (threshold crossing of local power), which are commonly used for the burst detection.

DOI: 10.1103/PhysRevD.76.103001 PACS numbers: 95.75.−z, 95.55.Ym, 04.80.Nn, 05.45.−a

I. INTRODUCTION

The noise in a physical apparatus affects not only the estimate of signal parameters but also the detection of the signal itself [1]. Very often, mathematical transformations (either linear or nonlinear) have to be applied to the sampled output of a detector to obtain further information that is not readily available in the raw samples. It was demonstrated that noise can enhance the detection of a weak periodic signal by means of bistable systems (stochastic resonance) [2]. However, how to boost the burst detectability through a suitably optimized nonlinear system, is still an open problem [3]. As an example, we consider the problem of detecting small signals buried in additive noise [i.e., at very low signal-to-noise ratio (SNR)], that has been thoroughly investigated in the field of gravitational wave searches [4]. If we assume signal sparsity and weakness, the output of a linear detector is normally dominated by its intrinsic noise sources, as prescribed by the fluctuation-dissipation theorem [5]. Deviations from Gaussianity, in particular, frequency subbands and/or specific time intervals can be handled by conditioning algorithms, such as bandcut filters or epoch vetoes [6]. In this case, we could use zero-mean stationary white Gaussian stochastic process as a model for the noise that corrupts the signal at the detector data. Thus the classical approach to the signal detection is to maximize the likelihood ratio over the parameters of expected signal templates [7] and then to fix a detection threshold on this statistics. The detection threshold is simply established by the desired level of false alarm probability. The maximum likelihood is compared with the aforementioned threshold and a detection is announced whenever the threshold is crossed.

Other modern mathematical tools, such as wavelet transforms [8,9], denoising by universal thresholding [10], generalized entropies [11], etc. can be successfully employed for the detection of some class of transient signals. Regardless of the linearity of data transformations, the detection occurs by means of a nonlinear procedure, e.g. a threshold crossing of the test statistics [12].

In this paper we explore a completely different approach for the burst detection, which is based on nonlinear excitable systems. Excitability is a common feature of natural systems including neural cells, chemical reactions, climate dynamics, etc. Common to all excitable systems is the existence of one stable rest state and a threshold crossing which triggers a deterministic orbit in the phase space (firing). In the excitable model analyzed in this work, namely, the FitzHugh-Nagumo (FN) system, the firing state is reached by means of weak "external stimulus." The dynamics of the FN system can be tuned to the variance of the detector noise, by means of bifurcation parameter in order to control the number of noise-induced firings. The presence of a deterministic signal in the sto-

*Corresponding author.
marino@fi.infn.it

chastic background increases the firing probability depending on the signal energy but irrespective to its waveform. We can profit from these unique features of excitable systems to implement a detection algorithm that identifies pieces of data where some sample amplitudes are incompatible with spontaneous fluctuations of the detector noise.

The presence or absence of a signal in the detector output affects the statistical characteristics of the observed data set. Thus the problem of signal detection can be conveniently reduced to a classical "hypothesis testing": on the basis of the observed data, we have to take our decision whether to reject or fail to reject the null hypothesis (the signal is absent) against the alternative hypothesis (the signal is present) [1,12]. As usual, we define the false alarm (P_{FA}) and detection (P_D) probabilities, respectively, as the probability to decide that the signal is present when it is absent and the probability to identify a signal when the signal is present. Useful graphical representations of P_D vs P_{FA} are the receiver operation characteristic (ROC) curves [13], which provide a systematic way of evaluating the performance of different detection algorithms.

The plan of the paper is as follows. In Sec. II we shortly review the dynamics of the excitable FN model. In Sec. III we describe the FN algorithm we have implemented and its potentialities for the bursts detection. In Sec. IV we study the performances of the FN algorithm by means of a Monte Carlo simulation of a detector output where detector noise is modeled by stationary stochastic process, and signals are drawn from the manifold of maximum entropy chirplets. We make also a comparison with the performances of power detectors. In Sec. V a conclusion is given and future research potentials of FN algorithm, extended to a detector network, are discussed.

II. DYNAMICAL MECHANISM OF EXCITABILITY

Excitable systems have a single stable fixed point and display a thresholdlike response to external perturbations: for stimuli above a certain threshold the system recovers its initial state following a deterministic orbit in the phase space (excitable response). These orbits appear in the system output as large pulses whose amplitude and duration depend only on the phase-space structure, while they are completely independent of the details of the external stimulus. This property makes these systems an interesting candidate as robust (i.e. independent of the perturbation characteristics) event trigger generators (ETGs) for detectors.

One of the most popular examples of excitability is provided by the FN system [14]:

$$\dot{x} = y + x - \frac{x^3}{3} \equiv y - f(x), \tag{1a}$$

$$\dot{y} = -\varepsilon(x - a), \tag{1b}$$

where $\dot{x}$ and $\dot{y}$ indicate the time-derivative of the real variables x and y. In this model, the variables x and y evolve with two very different characteristic time scales whose ratio is the parameter $\varepsilon \ll 1$.

The system possesses only one steady state solution $(x, y) = (a, \frac{a^3}{3} - a)$ [the intersection of the nullclines $x = a$; $y = f(x)$ in Fig. 1(a)] which is found to be stable for $|\, a \,| > 1$ and unstable otherwise. In this latter situation, the temporal dynamics of the system can be visualized in the limit $\varepsilon \to 0$ (singular perturbation analysis). In this limit, the evolution of the y variable is much slower with respect to that of the other variable x, therefore the dynamics of the complete system consists of fast and slow motions [15]. By setting $\varepsilon = 0$ in Eq. (1b), we can see that the fast motion evolves accordingly with Eq. (1a) (fast subsystem), where y is now a constant parameter. On the other hand, by introducing the slow time scale $\tau = \varepsilon t$ and setting $\varepsilon = 0$, we obtain the slow subsystem equation $\dot{y} = a - x$, with the constraining condition $y = x^3/3 - x$. Hence, the slow motion in the phase space is limited to trajectories taking place on the curve $\Sigma = \{(x, y) \in \{y = f(x)\}\}$ (slow manifold). Note that Σ consists of fixed points of the fast subsystem: these points are unstable if $x^2 < 1$ while they are stable if $x^2 > 1$. Then, regardless of what value y is fixed, the solution of the fast subsystem will rapidly approach one of the branches of stable points, $\Sigma_1 = \Sigma \cap \{x > 1\}$ and $\Sigma_2 = \Sigma \cap \{x < -1\}$. We now allow y to slowly vary accordingly with the equation $\dot{y} = a - x$. Close to $\Sigma_{1,2}$ we have attracting trajectories, while close to the unstable branch we have repelling trajectories. The flow direction on the slow manifold is given by the sign of $\dot{y}$ which is positive if $x < a$ and negative otherwise and is indicated by the arrows in Fig. 1(a). At this point we have all the

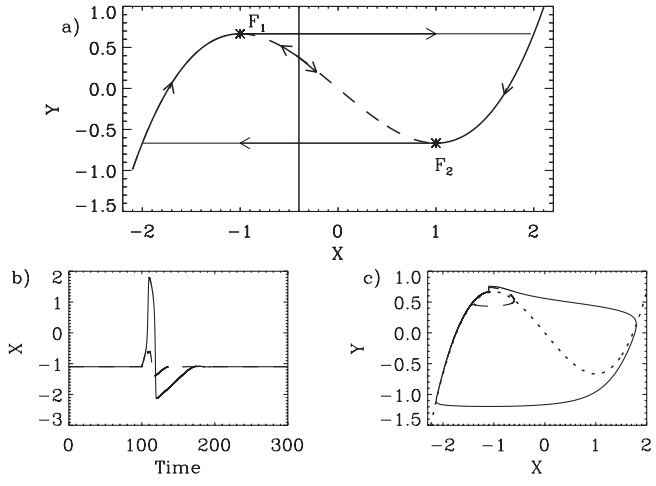

FIG. 1. (a) Nullclines of Eqs. (1) and flow directions on the slow manifold $y = f(x)$ for $a = -0.4$ in the limit $\varepsilon = 0$. The stars indicate the fold points separating the stable and unstable branches of the slow manifold. (b) Response of the FN system ($a = -1.1$) to a δ-like perturbation of amplitude $p_0 = 0.09$ (dashed line) and $p_0 = 0.1$ (solid line). (c) The corresponding phase-space trajectory compared with the slow manifold (dotted line).

information we need in order to understand the dynamics of Eqs. (1). The fixed point of the complete system is given by the intersection between Σ and the curve $x = a$. When $a^2 < 1$ the curve $x = a$ intersects the repelling part of the slow manifold [as in the case depicted in Fig. 1(a)] and the fixed point is unstable as stressed by the outward arrows indicating the flow direction on the slow manifold. In this case we also have a stable limit cycle. A trajectory starting close to an attracting branch of the slow manifold must follow it until one of the fold points $\mathbf{F}_{1,2} = (\mp 1, \pm\frac{2}{3})$ is reached. Beyond this point the slow manifold is repulsive and the flow is pushed out of the slow manifold instantaneously jumping to the other attracting branch. Then it flows along this branch until the other fold point where it jumps back, and the system evolves on a limit cycle [16].

The phase-space structure and the slow-fast dynamics above described is the responsible of the key property (for our purposes) of our system, i.e. excitability. When $a^2 > 1$, i.e., when the curve $x = a$ intersects $\Sigma_{1,2}$, the fixed point is stable. However, the system can be excited, i.e., forced to temporarily jump to the branch which does not contain the fixed point, in response to a sufficiently strong perturbation; indeed, the effect of a perturbation $i(t)$ is somehow equivalent to instantaneously shifting the fixed point towards the repelling part of the slow manifold beyond the fold points $y = \pm 2/3$, where the jumps take place. Then, the system will jump to the opposite branch following it until the fold point and then it will recover its stable rest state [Figs. 1(a) and 1(b)]. In our scheme a ''detection'' of a stimulus $i(t)$ (i.e. a noisy signal) simply corresponds to this deterministic orbit in the phase space that we call firing. There is a threshold value for a perturbation amplitude below which excitations cannot occur for any stimulus duration [see Figs. 1(b) and 1(c)]. Moreover, for each amplitude above this threshold there is still a minimum value of duration which produces excitation: this is the time it takes the system to go from the fixed point to the jump point. Therefore, there is an amplitude-duration threshold curve for excitatory pulses. However, in the limit case in which the perturbation $i(t)$ can be well approximated by an impulsive (or δ-like) positive function, there is only a threshold for the perturbation mean value $\bar{I} \equiv \int i(t)dt$ [16]. The a_{cr} threshold is the minimal distance that the system should be pushed away from the fixed point in order to make it jump to the opposite branch. If $\varepsilon \ll 1$, this value is close to $\frac{2}{3} - |a - \frac{a^3}{3}|$. Figures 1(b) and 1(c) show the system response in the presence of both subthreshold (dashed line) and above-threshold (solid line) perturbations and the corresponding phase portrait compared to the slow manifold.

A deeper view of the transition mechanism is achieved by studying the stochastic version of the FN system by assuming that the stimulus is a deterministic signal superimposed to a stochastic process. The Langevin equations of a stochastic FN system read

$$\begin{aligned} dx &= [y - f(x)]dt \\ dy &= -\varepsilon(x - a)dt + h(t)dt + \sigma dw, \end{aligned} \tag{2}$$

where $h(t)$ is a possible deterministic contribution to the stimulus, dw is a Wiener-Levy process, and σ is its drift coefficient. It is worth noticing that in the δ-like approximation of the stimulus, the deterministic signal $h(t)$ can be recast into suitable initial conditions of Eq. (2). The corresponding Fokker–Planck equation for the transition probability P_{FP} density is not tractable analytically. However, one can study the dynamics of cumulants of P_{FP} in particular regimes; in fact, it has been demonstrated that, before and after the firing, $x(t)$ and $y(t)$ are approximately jointly normally distributed [17]. Within the Gaussian approximation, the system of cumulant equations involves only the first- and second-order cumulants. The approximate equations for the time evolution of means m_x and m_y, variances s_x and s_y, and covariance c_{xy} read [18]

$$\begin{aligned} \dot{m}_x &= -m_x^3/3 + m_x + m_y - m_x s_x \\ \dot{m}_y &= -\varepsilon(m_x - a) + h(t) \\ \dot{s}_x &= 2s_x(1 - m_x^2 - s_x) + 2c_{xy} \\ \dot{s}_y &= -2\varepsilon c_{xy} + \sigma^2 \\ \dot{c}_{xy} &= -\varepsilon s_x + s_y + c_{xy}(1 - m_x^2 - s_x), \end{aligned} \tag{3}$$

with initial conditions $m_x(0) = a$, $m_y(0) = a^3/3 - a$, $s_x(0) = 0$, $s_y(0) = 0$, and $c_{xy}(0) = 0$. Thus, the Langevin equations (2) are now approximated by a set of five nonlinear ordinary differential equations. Equations (3) can be further simplified by recognizing the difference in the relaxation time scales between the means and the variances: the former change slower than the latter. The onset of the stationary solution for variances and covariance is immediate compared with the time-scale ratio ϵ and so we can make use of their approximate stationary solution

$$\begin{aligned} s_x &= \sigma^2/[2\varepsilon(a^2 - 1)] \\ s_y &= \sigma^2[\varepsilon + (a^2 - 1)^2]/[2\varepsilon(a^2 - 1)] \\ c_{xy} &= \sigma^2/(2\varepsilon) \end{aligned} \tag{4}$$

to evaluate the evolution of the FN system. In addition, we can substitute the above stationary solution in the first two equations in the set of Eq. (3) to study the equilibrium point of the system. The stability analysis shows that the equilibrium point experiences a Hopf bifurcation with increasing ratio σ^2/ε and that the stability can be achieved by the intuitive requirement $\sigma^2/\varepsilon < 1$. From now on we require our FN system to operate in the stable regime by a suitable tuning of its parameter values.

The firing probability of a stable stochastic FN system can be obtained after the integration of the joint normal transition probability over all values of the variable y. Within the Gaussian approximation, the following expression gives a good approximation to the probability that the

stochastic process $x(t)$ is above a level θ

$$\mathcal{P}(\theta, t) = \frac{1}{2}\left[1 - \mathrm{erf}\left(\frac{\theta - m_x(t)}{\sqrt{2 s_x(t)}}\right)\right], \tag{5}$$

where $\mathrm{erf}(x)$ is the error function. It is worth noticing that even though $\mathcal{P}(\theta, t)$ can be evaluated from $m_x(t)$ and $s_x(t)$, the determination of these two quantities requires the solution of all five of Eqs. (3). However, at early times $[t < O(\varepsilon^{1/2})]$, during the prefiring dynamical evolution of the FN system, we have that $m_x \simeq a$ and $m_y \simeq a^3/3 - a$ plus terms involving the deterministic signal. During this regime, the firing probability is stationary and depends on the mean value of noise and signal in the stimulus $\bar{i}$, and hence the FN system can be successfully employed as a detector of transient signals. Moreover, we are able to assess the detection of a signal $h(t)$ by a standard hypothesis testing and decide to reject the null hypothesis $\{\mathcal{H}_0$: "absence of a signal in T"$\}$ when the FN system exhibits a firing. If ε is as small as 10^{-2}, the period T can be long enough to detect transient signals of 0.1 s which represents the expected duration of gravitational wave (gw) bursts [19]. In the absence of deterministic signals $[h(t) = 0]$, the stationary firing probability for time intervals of duration $T < O(\varepsilon^{1/2})$ reads

$$P_\varepsilon(a) = \tfrac{1}{2}\{1 - \mathrm{erf}[(a - a_{\mathrm{cr}})\sqrt{\varepsilon(a^2 - 1)/\sigma^2}]\}, \tag{6}$$

where $\mathrm{erf}(x)$ is the error function and a_{cr} is the critical threshold to make a transition from the steady to the firing state. From slow manifold analysis, one can also show that the critical threshold for the x variable to produce a firing is given by $a_{\mathrm{cr}} = -1 + O(\varepsilon)$. If we reset the FN system at the beginning of each window of a given duration T [i.e. by setting $m_x(kT) = a$, $m_y(kT) = a^3/3 - a$ and $k = 1, 2, 3 \ldots$], we can analyze longer stimulus duration and evaluate analytically the false alarm rate (FAR); in this case, the threshold crossing of $x(t)$ for a pure stochastic stimulus is nothing but a stationary Poisson process with rate $\mathrm{FAR} = P_\varepsilon(a)/T$ [20].

III. DETECTION ALGORITHMS BY NONLINEAR FN SYSTEMS

To apply the FN detection algorithm to a data set collected by some physical apparatus, firstly we have to specify Eqs. (2) in the discrete time domain by choosing a suitable sampling time Δt. It is worth noticing that Δt has to be lower than the inverse of the signal bandwidth (Nyquist theorem) and it must allow, at the same time, an accurate integration of the nonlinear dynamics of FN system. Throughout the following, a subset of observed data, i.e. the stimulus, consist of N_s samples $i_k = (h_k + n_k)^2$ $(k = 1 \ldots N_s)$, where the signal h_k is unknown and the noise n_k is a discrete realization of a white, stationary, and Gaussian stochastic process with zero mean and variance σ^2. In practice, assuming that the noise power spectral density is constant over a bandwidth $B/2$, we have $n_k = B^{-1/2}\sigma N_k$, where $\{N_k\}$ is a sequence of independent and identically distributed standard normal random variables, obtained from computer library routines. We decide to square the detector data with a twofold effect: (i) to relax the Gaussian assumption for the detector noise; and (ii) to have larger positive fluctuations and so to profit of the asymmetric FN dynamics. In addition, we assume that the complete data set to be analyzed can be divided in subsets that may contain only one signal, but completely. In all practical cases (in particular for the detection of gw bursts), the above requirements are easily met as soon as signals are sparse and time limited. The simulation scheme of our detection algorithm consists of the recursive relations

$$\begin{aligned} x_{k+1} &= x_k + \Delta t[y_k - f(x_k)] \\ y_{k+1} &= y_k - \Delta t[\varepsilon(x_k - a) + i_k], \end{aligned} \tag{7}$$

where $x(k\Delta t)$ and $y(k\Delta t)$ are approximated by x_k and y_k respectively. The value of Δt was pragmatically fixed to 10^{-4} s, the value being determined by our aim to solve Eqs. (7) in the presence of stimuli drawn from the parameter subspace of chirplet signals that could represent gw bursts. We also choose $\varepsilon = 0.07$ and $\sigma = 0.3$ which ensures that the system is in its excitable stable state. The initial conditions, which correspond to the stationary solution of Eqs. (7), read $x_0 = a$, $y_0 = a^3/3 - a$; the system is then evolved for times much larger than the stimulus duration T, looking for its eventual firing.

IV. MONTE CARLO SIMULATIONS

A. Spontaneous firing

To study the spontaneous firing probability we estimate the empirical number of the "spontaneous firings" of the FN system, i.e. the false alarms of the FN detector. The Monte Carlo ensemble consists of 10^5 noise stimulus of $N_s = 10^3$ samples (0.1 s duration) fed to the recursive relations of Eq. (7). As the initial conditions reset the FN system each time a stimulus is analyzed, the resulting statistics of firing times is "*a fortiori*" a Poisson process. The false alarms, being independent of signals, have been determined with a good accuracy at any interesting rate. In Fig. 2 we plot the empirical number of firings of FN detection algorithm as a function of the parameter a. Such a false alarm curve cannot be easily calculated since the detector data have been squared and the stochastic term is no longer zero-mean Gaussian noise. However, it can be still approximated by Eq. (6), obtained in the Gaussian noise approximation, provided that the fitting parameters are suitably chosen (see Fig. 2).

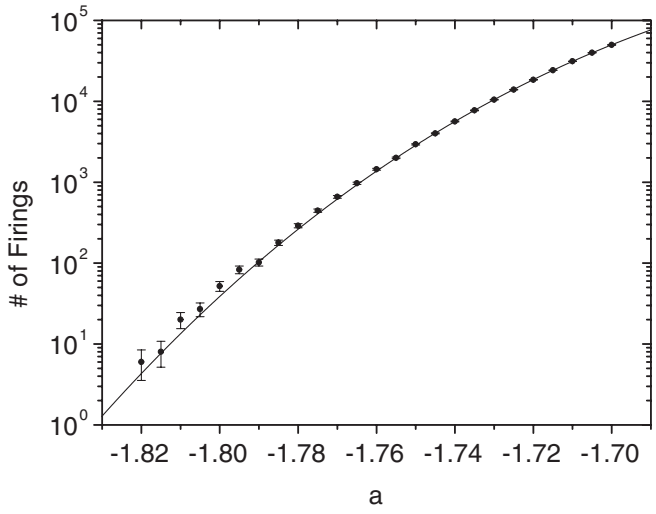

FIG. 2. Number of noise-induced firings as a function of the control parameter a. The continuous line is the plot of the fitting function $\Lambda_1\{1 - \mathrm{erf}[(a - \Lambda_2)\sqrt{\Lambda_3(a^2 - 1)}]\}$ with best fit parameters $\Lambda_1 = 6.05 \times 10^5$, $\Lambda_2 = 1.61$, and $\Lambda_3 = 99.0$.

B. Detection of chirplet signals

We now show the results of numerical simulations carried out on the FN discrete model of Eqs. (7) by adding a deterministic burst signal to its stimulus. The detection procedure is very simple: we consider again windows of $N_s = 10^3$ samples as stimulus; the firing of the associated FN system is now employed as a binary classifier for the presence vs the absence of a deterministic signal in the stimulus. The corresponding ROC curves [13] of the FN detection algorithm can be estimated by varying the control parameter a. To evaluate its detection efficiency P_D, we decided to inject maximum entropy chirplets, which perform as a sort of reference burst signal adopted for instance in gravitational wave searches. Chirplets are a class of nonstationary signals defined in a six-parameter space

$$h(t) = \frac{h_{\mathrm{rss}}}{\sqrt[4]{2\pi\Delta_\tau^2}} \exp\left[-\frac{(t - t_0)^2}{4\Delta_\tau^2}\right] \times \cos\left[\frac{\beta}{2}(t - t_0)^2 + \omega_0(t - t_0) + \phi_0\right], \quad (8)$$

where $h_{\mathrm{rss}}^2 \equiv \int h^2(t)dt$ is the chirplet energy (i.e. the root-sum-square (rss) of the chirplet samples in Hz^{-1} units), t_0, Δ_τ, ω_0, and Δ_ω are arrival time, duration, central frequency, and bandwidth of the chirplet; here $\beta \equiv (\Delta_\omega/\Delta_\tau)\sqrt{1 - (2\Delta_\tau\Delta_\omega)^{-2}}$ is the chirp rate and ϕ_0 is an arbitrary initial phase. Chirplets have quite a varied signature in the time-frequency plane and a maximum entropy [21]. Other remarkable properties of the chirplet waveforms are the following: (i) covariance to scale changes of Δ_ω, chirp rate β, time of arrival t_0, and central frequency ω_0 (a very desirable property to study a detection algorithm); (ii) satisfy the uncertainty principle with equality when $\Delta_\omega\Delta_\tau = \frac{1}{2}$; (iii) attain a good resolution in both time and frequency; (iv) "sin-Gaussian" waveforms can be recovered as the particular case $\beta = 0$. In our Monte Carlo simulations, the injected chirplets were drawn from uniform probability distributions over the parameter subspaces $\mathcal{M}$ defined as follows: $10^{-3} \le \Delta_\tau \le 10^{-2}$ s (i.e. transient signals); $10 \le \Delta_\omega/(2\pi) \le 10^2$ Hz, $500 \le \nu_0 \le 1000$ Hz and $0 < \phi_0 \le 2\pi$. Bandwidth and duration were chosen in accordance with the Heisenberg lower bound $\Delta_\omega\Delta_\tau \ge 1/2$ [22] as clearly illustrated by the presence of the black region in Fig. 3. To avoid synchronizations among sampling process, detection algorithms and injected signals, we add a random jitter of values randomly chosen between ± 2.5 ms to the arrival time t_0 relative to the center of the window. The signal-to-noise ratio of injected chirplets is calculated as $\mathrm{SNR} = h_{\mathrm{rss}}B^{1/2}/\sigma$, and it corresponds to the maximum SNR achievable by the ideal matched filter [20]. In the following we assume $B = 2$ kHz as the order of magnitude of the bandwidth of operating gw detectors [23].

First, we studied the robustness of the FN detection algorithm; to this aim we generated $N \sim 2 \times 10^7$ independent data windows for nine couples of three FARs (8×10^{-5}, 9.9×10^{-4}, and 9.7×10^{-3} Hz) and three SNRs (7.5, 8.5 and 9.5). We then partitioned the data into 10^4 sets of L_k chirplets each. These sets corresponds to 100×100 $(\Delta_\omega, \Delta_\tau)$ cells, as clearly illustrated in Fig. 3; note that the number of cells compatible with the Heisenberg principles is $\sim 8 \times 10^3$.

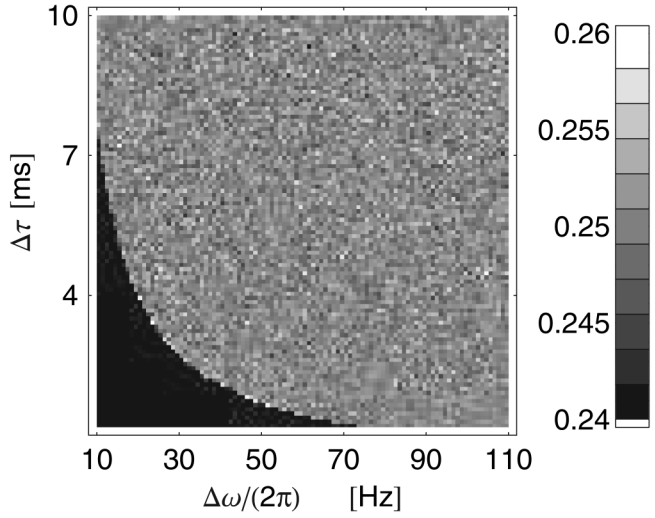

FIG. 3. The detection efficiency of FN algorithm over the bandwidth Δ_ω and duration Δ_τ parameter space. SNR and FAR are 7.5 and 10^{-3} Hz, respectively. The black region is forbidden by the Heisenberg uncertainty principle; its area is $\sim$20% of the area of the whole time-frequency rectangle (see text).

TABLE I. Average detection probabilities $P_{D\mathcal{M}}$ and standard deviations $\sigma_{\mathcal{M}}$ calculated at three different values of FAR and SNR over the chirplet submanifold $\mathcal{M}$.

FAR\SNR	7.5	8.5	9.5
9.7×10^{-3} Hz	0.4661 ± 0.013	0.7552 ± 0.010	0.9370 ± 0.005
9.9×10^{-4} Hz	0.2636 ± 0.009	0.5591 ± 0.011	0.8397 ± 0.010
8.0×10^{-5} Hz	0.1184 ± 0.007	0.3449 ± 0.008	0.6738 ± 0.011

The average number of injected chirplets in each cell is $\sim 2 \times 10^3$ with a square-root statistical fluctuation. Because of the Heisenberg uncertainty relations, there are few cells cut by the $\Delta_\omega \Delta_\tau = 1/2$ curve. As these cells have larger statistical fluctuations ($L_k \ll 10^3$), we decided to remove them from the robustness analysis of FN detection algorithm. Each efficiency measurement consists in a number of observations representing one of two possible outcomes "accept" or "reject" the null hypothesis $\mathcal{H}_0$. Thus, the statistic variable F_k, representing the number of firings in each cell, obeys the binomial distribution which gives the probability of observing F_k successes in L_k trials [20]. One can easily show that the maximum likelihood estimator of P_D is the ratio $P_{Dk} = F_k/L_k$ with a variance $\sigma_k^2 = P_{Dk}(1 - P_{Dk})/L_k$. For large sample size [i.e. $P_{Dk} \times L_k > 10$ and $(1 - P_{Dk}) \times L_k > 10$] the binomial distribution can be approximated by a Gaussian distribution with mean $L_k P_D$ and variance $\sigma_k^2 = L_k P_D (1 - P_D)$. The relative error on the efficiency estimate in each cell is then of the order of $P_{Dk}/\sigma_k \approx F_k^{-1/2} < 0.01$ for all the $\sim 8 \times 10^3$ cells we considered. Since this value is very small, we can study the dependence of local efficiency on cells by looking at the deviation of P_{Dk} from the average efficiency $P_{D\mathcal{M}} = \langle P_{Dk} \rangle_{\mathcal{M}}$ over the submanifold $\mathcal{M}$ as an indication of robustness of the algorithm. We estimated $\sigma_{\mathcal{M}} \equiv \langle (P_{Dk} - P_{D\mathcal{M}})^2 \rangle_{\mathcal{M}}^{1/2}$ as the rms of the efficiency fluctuations around its mean value. The values reported in Table I represent the average detection efficiency over the entire chirplet submanifold $\mathcal{M}$. From Table I we see also that $\sigma_{\mathcal{M}} \approx 0.01$. Moreover, if detection probabilities are constant, the errors on their average are $\simeq 1/\sqrt{8 \times 10^3} \simeq 1.1 \times 10^{-2}$ smaller than the reported standard deviations. Thus we are able to accurately compare each averaged detection probability $P_{D\mathcal{M}}$ with the ratio of the total number of firings and the total number of data windows for each entry in Table I. We found no significative differences between the two estimates and we conclude that the FN detection efficiency is constant over $\mathcal{M}$. The analysis in Sec. II entails that the achieved results are independent of the choice of chirplets as reference signals for testing our implementation of the FN algorithm.

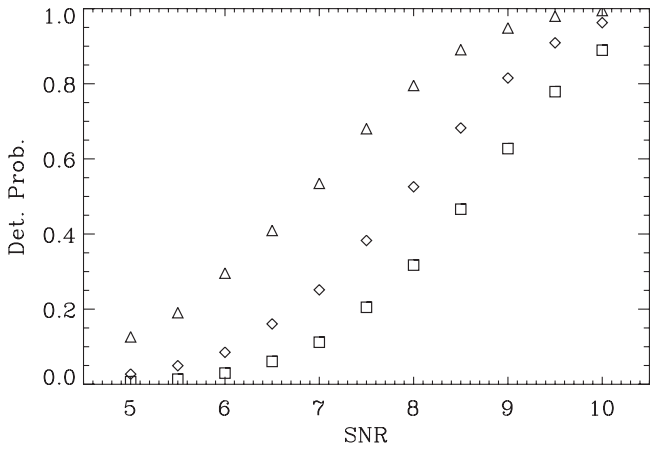

FIG. 4. Detection efficiencies P_D as a function of SNR for three different FARs: 10^{-3} (squares), 10^{-2} (diamonds), and 10^{-1} Hz (triangles).

Having established the robustness of the FN algorithm we proceed to investigate its detection efficiency and we defer the discussion of ROC curves to the next section. To this aim, we apply to 10^5 independent noisy data sets the FN algorithm with control parameter values corresponding to FARs 10^{-3}, 10^{-2}, and 10^{-1} Hz, where a more sensitive dependence on the SNR is expected. We pick up one cell of Fig. 3 representing a chirplet with duration $\Delta_\tau = 0.01$ s, bandwidth $\Delta_\omega/(2\pi) = 100$ Hz, and central frequency 800 Hz. The sigmoid-type behavior of the detection efficiency is clearly visible in Fig. 4 where we report the estimated P_D as a function of SNR.

C. Power based detection algorithms

To make a comparison of FN with other detection algorithms, we briefly discuss the performances of classical power detectors based on the square of samples. The interest in power detectors resides in the fact that localized power of a data set i_k can be used to form a robust statistics for the detection of transient signals [1,24]. In addition, by means of suitable filters we are able to perform a uniformly most powerful test on the localized power statistics [24] defined as

$$\mathcal{E}_q = \sum_k (q \circ i)_k / \sigma^2, \tag{9}$$

where $\circ$ is the convolution operator and $q(t_0, \omega_0, \Delta_\tau, \Delta_\omega)$ is a filter that selects the box of the time-frequency plane where (most of) the signal power is concentrated. Thus the decision rule for a power filter detection algorithm (PF) can be stated as "if $\mathcal{E}_q > \xi$ we reject the null hypothesis $\mathcal{H}_0$," where ξ is a threshold fixed by the desired level of FAR.

Unfortunately, the construction of an optimal statistics requires the "*a priori*" knowledge of the time-frequency box $(t_0, \omega_0, \Delta_\tau, \Delta_\omega)$ with a consequent weakening of robustness requirements. Suboptimal approaches for the transient detection consist in suitable families of q filters (for example wavelet bases) which allow a restriction of the sum in Eq. (9) to particular index clusters, defined for instance by threshold crossing of addends $(q \circ i)_k$. The power statistics will depend on the effective number $N_{\rm eff}$ of independent squared samples which contributed to $\mathcal{E}_q$ and the amount of signal E_q collected by the filters q, i.e. $E_q = \sum_{k=1}^{N_{\rm eff}} (q \circ h^2)_k \propto h_{\rm rss}^2$.

While having Gaussian additive white noise in the stimulus i_k, the local power $\mathcal{E}_q$ obeys the noncentral χ^2 distribution with noncentral parameter equal to E_q/σ^2 [9]; this distribution cannot be expressed with elementary functions. However, in the limit of large $N_{\rm eff}$, the noncentral χ^2 cumulative distribution function can be calculated by the two-moment approximation [25], and the ROC curves of PF detectors can be written in a useful form

$$\begin{cases} P_{\rm FA}(\xi) = \gamma(\frac{N_{\rm eff}}{2}, \frac{\xi}{2})/\Gamma(\frac{N_{\rm eff}}{2}) \\ P_D(\xi) = \gamma(g_1 \frac{N_{\rm eff}}{2}, g_2 \frac{\xi}{2})/\Gamma(g_1 \frac{N_{\rm eff}}{2}), \end{cases} \tag{10}$$

where $\gamma(x, y)$ and $\Gamma(x)$ are the incomplete and complete Euler Gamma functions, ξ is the threshold controlling the FAR, $g_1 \equiv (1+\alpha)^2/(1+2\alpha)$ and $g_2 \equiv (1+\alpha)/(1+2\alpha)$; here $\alpha \equiv (E_q/N_{\rm eff})/\sigma^2$ represents the ratio between the time averaged energy of the signal and the noise variance. It is worth noticing that for $\alpha < 0.1$ (i.e. in the low SNR regime) $g_1 \simeq 1 + O(\alpha^2)$ and $g_2 \simeq 1 - \alpha + O(\alpha^2)$.

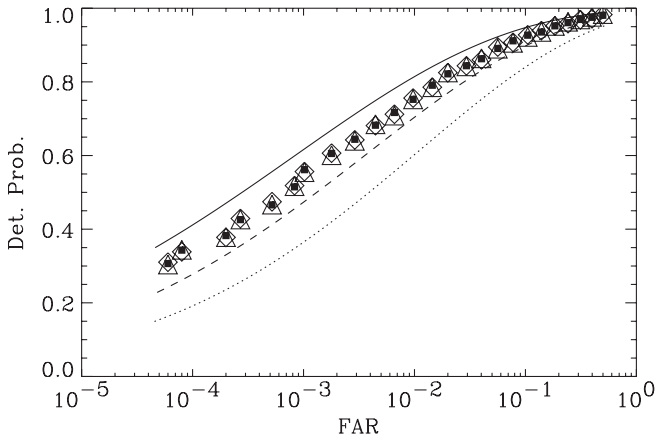

FIG. 5. ROC curves for the PF and FN (symbols) detectors for SNR = 8.5 signals. Durations and bandwidths of the injected chirplet are $\Delta_\tau = 0.01$ s and $\Delta_\omega/(2\pi) = 10$ Hz (triangle), $\Delta_\tau = 0.001$ s and $\Delta_\omega/(2\pi) = 100$ Hz (solid square), and $\Delta_\tau = 0.01$ s and $\Delta_\omega/(2\pi) = 100$ Hz (diamond). The three curves correspond to the ROCs of a power detector with $N_{\rm eff} = 800$ (continuous line), $N_{\rm eff} = 1000$ (dashed line), and $N_{\rm eff} = 1200$ (dotted line).

For the comparison of FN and PF detection algorithms we assume a trivial power filter. The resulting statistics $\mathcal{E} = \sum_{k=1}^{N_{\rm eff}} i_k$ is no longer optimal but it becomes independent of signal waveforms as long as signals is completely contained in the window, and so a fair comparison with the FN performances is possible. We report in Fig. 5 some ROC curves we have obtained in 10^5 trials by injecting SNR = 8.5 chirplets with central frequency $\omega_0/(2\pi) =$ 800 Hz, and located in three very different positions of the time-frequency plane. We note the complete superposition of the three curves over four orders of FAR magnitude. With the intent of figuring out the relative performances of FN and PF detection algorithms we also plot in Fig. 5 the curves in Eqs. (10) relative to a power statistics with three different effective number of samples.

V. CONCLUSIONS

In this work we have presented a viable alternative to the classical detection procedure based on a threshold crossing of a suitable statistics. In particular, our detection scheme, based on the firing of a FN system, does not require "*a priori*" hypothesis on amplitude, arrival time or waveform patterns. The FN detection algorithm is quite general and can be applied to narrow or wide band detectors once the requirements of noise quasistationarity and signal sparsity are fulfilled.

To calculate the detection efficiency of the FN algorithm, we have explored the six dimensional chirplet parameter space $\mathcal{M}$; however, the singular perturbation analysis in Sec. II clearly indicates that the results we get are independent of waveforms as long as analyzed stimulus containing only one burst, but completely (signal sparsity) and signal bandwidth do not exceed the detector bandwidth B. The obtained ROC curves show that the FN algorithm can be successfully employed as a robust detector of transient signals, and that its overall efficiency is comparable with the efficiency of power based detection algorithms. However, the FN algorithm is more tunable as it depends from the dynamical threshold a, which set the FAR, and on the time-scale variable ε, which soften the threshold behavior. Of course, the achieved robustness with respect to signals variability entails the absence of peaks and valleys in the detection efficiency while detection algorithms that make "*a priori*" assumptions on signal waveforms must have higher but nonuniform efficiency. We think that the FN detector is quite insensitive to the noise statistics as we square the stimulus and, despite the statistics is no longer Gaussian, the dependence of false alarms on a can still be fitted by Eq. (6). However, much work has still to be devoted to analyzing the robustness of FN with respect to noise statistics.

The main motivation for the present study regards the possibility to implement arrays of coupled FN systems

devised for applications to networks of gw detectors. Indeed, excitable systems can be coupled and synchronized by means of suitable either linear and nonlinear feedback terms. These arrays of self-controlled detection algorithms should lead to a dramatic reduction of the FAR keeping the detection efficiency basically unchanged. The implementation of distributed detection algorithms based on arrays of FN systems—together with its application to more realistic gw data—will be the subject of a future work.

[1] C. W. Helstrom, *Statistical Theory of Signal Detection* (Pergamon Press, Oxford, 1968).

[2] L. Gammaitoni *et al.*, Rev. Mod. Phys. **70**, 223 (1998); A. R. Bulsara *et al.*, Phys. Rev. E **67**, 016120 (2003);

[3] A. Dutta and G. P. Anand, in *TENCON 2004: Proceedings of the 2004 IEEE Region 10 Conference* (Chiang Mai, Thailand, 2004), Vol. A, p. 251.

[4] N. Arnaud *et al.*, Phys. Rev. D **59**, 082002 (1999); **67**, 062004 (2003); W. G. Anderson *et al.*, *ibid.* **63**, 042003 (2001); S. Mohanty, *ibid.* **61**, 122002 (2000); J. Sylvestre, *ibid.* **66**, 102004 (2002); N. Arnaud *et al.*, *ibid.* **67**, 062004 (2003); T. Pradier *et al.*, *ibid.* **63**, 042002 (2001); S. Klimenko *et al.*, Classical Quantum Gravity **21**, S1685 (2004); J. W. C. Mc Nabb *et al.*, *ibid.* **21**, S1705 (2004).

[5] See e.g. H. B. Callen and T. A. Welton, Phys. Rev. **83**, 34 (1951); J. Weber, Phys. Rev. **101**, 1620 (1956).

[6] P. Ajith, M. Hewitson, J. R. Smith, and K. A. Strain, Classical Quantum Gravity **23**, 5825 (2006); A. Di Credico *et al.*, *ibid.* **22**, S1051 (2005).

[7] See e.g. S. Babak *et al.*, Classical Quantum Gravity **23**, 5477 (2006); S. Babak, H. Grote, M. Hewitson, H. Lück, and K. A. Strain, Phys. Rev. D **72**, 022002 (2005); Y. Tsunesada *et al.*, Phys. Rev. D **71**, 103005 (2005).

[8] See e.g. M. Frish and M. H. Messe, IEEE Trans. Inf. Theory **38**, 892 (1992); S. Del Marco and J. Weiss, IEEE Trans. Signal Process. **45**, 841 (1997).

[9] M. Camarda and A. Ortolan, Phys. Rev. D **74**, 062001 (2006).

[10] For a wavelet based denoising with automatic noise level estimation, see e.g. D. L. Donoho, IEEE Trans. Inf. Theory **41**, 613 (1995).

[11] See e.g. R. G. Baraniuk *et al.*, IEEE Trans. Inf. Theory **47**, 1391 (2001).

[12] M. H. A. Davis, in *Proceedings of the NATO Advanced Research Workshop on Gravitational Wave Data Analysis*, edited by B. F. Schutz (Kluwer Academic Publishers, Dordrecht/Boston/London, 1989), p. 73.

[13] T. Fawcett, HP Laboratories, Palo Alto, CA, Technical Report No. HPL-2003-4.

[14] R. FitzHugh, Biophys. J. **1**, 445 (1961); J. Nagumo, S. Arimoto, and S. Yoshizawa, Proc. IRE **50**, 2061 (1962).

[15] M. W. Hirsch and S. Smale, *Differential Equations, Dynamic Systems and Linear Algebra*, Pure and Applied Mathematics Vol. 60 (Academic Press, New York-London, 1974).

[16] M. Feingold, D. Gonzalez, O. Piro, and H. Viturro, Phys. Rev. A **37**, 4060 (1988).

[17] H. C. Tuckwell and R. Rodriguez, J. Comput. Neurosci. **5**, 91 (1998).

[18] A. H. Jazwinski, *Stochastic Processes and Filtering Theory* (Academic Press, New York, 1970).

[19] See e.g. R. F. Stark and T. Piran, Phys. Rev. Lett. **55**, 891 (1985); H. Dimmelmeier, J. A. Font, and E. Müller, Astrophys. J. Lett. **560**, L163 (2001); C. D. Ott, A. Burrows, E. Livne, and R. Walder, Astrophys. J. **600**, 834 (2004).

[20] A. Papoulis, *Probability, Random Variables, and Stochastic Processes* (McGraw-Hill, Singapore, 1984).

[21] S. Mann and S. Haykin, IEEE Trans. Signal Process. **43**, 2745 (1995).

[22] The ratio between the area forbidden by the uncertainty principle $\int_{\omega_1}^{\omega_2} d\omega/(2\omega) = \ln(\omega_2/\omega_1)/2$ and the area of the $[\omega_1, \omega_2] \times [1/(2\omega_1), 1/(2\omega_2)]$ time-frequency rectangle can be approximated by $\simeq \log(\lambda)/\lambda$, where $\lambda \equiv \omega_2/\omega_1 > 1$. For the chirplet submanifold $\mathcal{M}$, $\lambda = 11$ and this ratio is $\simeq 0.23$.

[23] For the sensitivity curve of LIGO and VIRGO gw detectors, see e.g. D. Sigg (LSC), Classical Quantum Gravity **23**, S51 (2006); F. Acernese *et al.*, *ibid.* **23**, S63 (2006).

[24] W. G. Anderson *et al.*, Phys. Rev. D **63**, 042003 (2001); Int. J. Mod. Phys. D **9**, 303 (2000).

[25] P. B. Patnaik, Biometrika **36**, 206 (1949).